

LA-UR-21-28526

Approved for public release; distribution is unlimited.

Title: Penetrating power in radiography of high-Z materials as a function of bremsstrahlung spectrum endpoint energy

Author(s): Tobias, Benjamin John
Tomkins, Christopher David

Intended for: Report

Issued: 2021-08-26

Disclaimer:

Los Alamos National Laboratory, an affirmative action/equal opportunity employer, is operated by Triad National Security, LLC for the National Nuclear Security Administration of U.S. Department of Energy under contract 89233218CNA000001. By approving this article, the publisher recognizes that the U.S. Government retains nonexclusive, royalty-free license to publish or reproduce the published form of this contribution, or to allow others to do so, for U.S. Government purposes. Los Alamos National Laboratory requests that the publisher identify this article as work performed under the auspices of the U.S. Department of Energy. Los Alamos National Laboratory strongly supports academic freedom and a researcher's right to publish; as an institution, however, the Laboratory does not endorse the viewpoint of a publication or guarantee its technical correctness.

Penetrating power in radiography of high-Z materials as a function of bremsstrahlung spectrum endpoint energy

B. Tobias and C. Tomkins
P-23 Neutron Science and Technology

A modified radiographer's equation is derived and fitted to simulation data so as to describe the increase in radiographic signal that comes with increasing bremsstrahlung spectrum endpoint energy. The dose contained in the incident spectrum follows an $E^{2.8}$ power law, as often cited. However, the direct flux penetrating through a heavy, high-Z material, obeys a weaker scaling due to hardening of the radiation. The resultant expression depends on the thickness of the scene being radiographed, the composition of high-Z materials in the scene, and any filtering by other low-Z materials, such as Al or Be. The expression exhibits two asymptotic limits: a 'thick' limit at which radiation is extremely hardened and only a weak benefit to increasing endpoint energy is observed (also the most attenuating limit and therefore of dubious physical significance), and a 'thin' limit at which a minimum of high-Z material is present and the penetrating dose exhibits the 2.8 power scaling inherent in the incident spectrum. Behavior for intermediate thicknesses of W and Al are obtained by modeling incident and attenuated dose using the DOSECALC code and the Bayes' Inference Engine (BIE). These data guide the optimization of MeV radiography over a wide range of energies where pair production plays a significant role in photon scattering.

Introduction

Radiography of thick scenes containing high-Z materials requires photon energies in the multi-MeV range. At energies in excess of ~ 1 MeV, photoelectric and Compton cross-sections decrease enough to allow what is considered a useful fraction of dose to penetrate the material and arrive at the detection apparatus. Facilities such as PHERMEX [1] and DARHT [2], as well as that proposed by the ASD-Scorpius project [3, 4], radiograph heavy objects by accelerating electrons to well above 10 MeV and colliding them with a high-Z converter target to produce a bremsstrahlung photon spectrum with a high endpoint energy and significant dose between 1 and 4 MeV. In the optimization of a new system, one considers the trade-off between electron beam energy and current. It is well known that the total dose contained in a bremsstrahlung spectrum scales roughly as endpoint energy to the 2.8 power. However, the efficacy of dose in the high-energy range of the spectrum is somewhat reduced by the increase in the pair production cross section exhibited by high-Z materials of interest. The scaling of penetration, or the dose that arrives at the detector after attenuation by the scene, must be evaluated when specifying the electron beam energy and charge delivered to the converter.

In Figure 1 a), the total attenuation cross section of Ta is shown, on a linear scale, from 1 to 8 MeV. A minimum in the attenuation curve appears in the vicinity of 4 MeV. Here, radiation is most penetrating. Below this window, attenuation is dominated by Compton scattering. Above this window, the pair production cross-section increases steadily. This 'window' effect is a function of the atomic number, Z. Figure 1 b) compares the cross sections for 6 different elements. Those elements that exhibit a minimum in attenuation near 4 MeV are considered high-Z elements from the radiographer's perspective. Tungsten (Z=74) will be taken as an exemplar for much of the analysis that is to be presented.

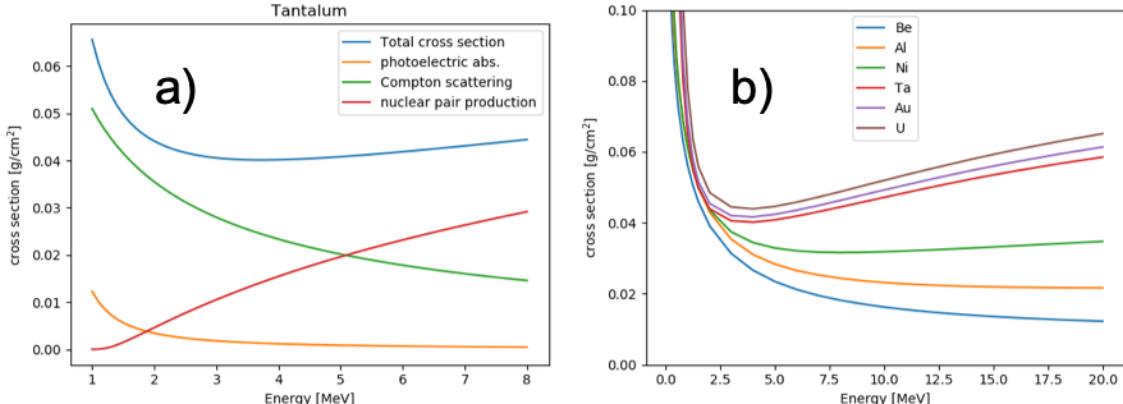


Figure 1. a) *Photon interaction cross-sections for Tantalum ($Z=74$).* Photoelectric absorption becomes insignificant in the region of interest, and Compton scattering reduces monotonically. However, pair production in the nuclear field increases steadily, making for a monotonic increase in the total cross section above 4 MeV. b) ‘Windowing,’ or exhibiting a minimum in the total cross section at a few MeV, is a feature common to high-Z materials that are often of interest for radiography.

Figure 2 presents several bremsstrahlung spectra produced by mono-energetic electron beams with energies above the minimum of the W attenuation curve. They are labeled by the mean photon energy of the spectra. As endpoint energy increases, the mean energy at first becomes more penetrating. Increasing further, more and more photon energy is introduced in a range where it is likely to be converted by pair production and subsequent interactions to electrons or secondary photons, i.e. scatter. That scattered radiation is eventually captured by photo-electric events in the material or escapes in a manner that is no longer useful for imaging the scene. It is therefore clear that, although increasing the electron beam energy delivers more flux to the material being imaged, an increasingly large fraction of that additional energy is being attenuated. There is still advantage in going to the highest energies, but it is not as great as suggested by a 2.8 power scaling.

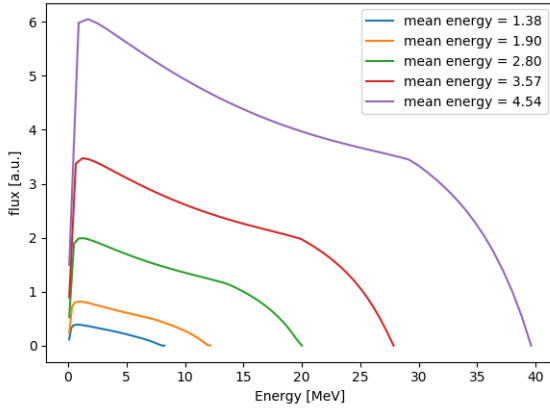


Figure 2. Bremsstrahlung spectra produced by increasingly energetic electron beams.

The actual scaling of useful, penetrating, un-collided, or direct flux as a function of endpoint energy depends on the scene to be radiographed. Specifically, it depends on the amount of high-Z material present to harden the spectrum and reduce the efficacy of the highest energy photons. Data for understanding this relationship and fitting coefficients is produced by modeling the bremsstrahlung spectrum with the DOSECALC script [5], and then attenuating that spectrum according to Beer’s Law. Exponential attenuation is combined with the detector response of DARHT and DARHT-like detectors within the Bayes’ Inference Engine (BIE) [6]. This code also integrates the detected spectrum to provide a relative signal level, or image intensity for a

given scene. These relative intensities are then compared to each other in order to provide a scaling that is to be fit with a functional form. Figure 3 presents some of this data, normalized by the assumption that probing 140 g/cm² of W with a 19.6 MeV endpoint bremsstrahlung spectrum produces 25 mR of direct photon dose at the detector. 40 g/cm² of Al filter is assumed in each case, and the amount of W in the scene is varied from 80 to 320 g/cm².

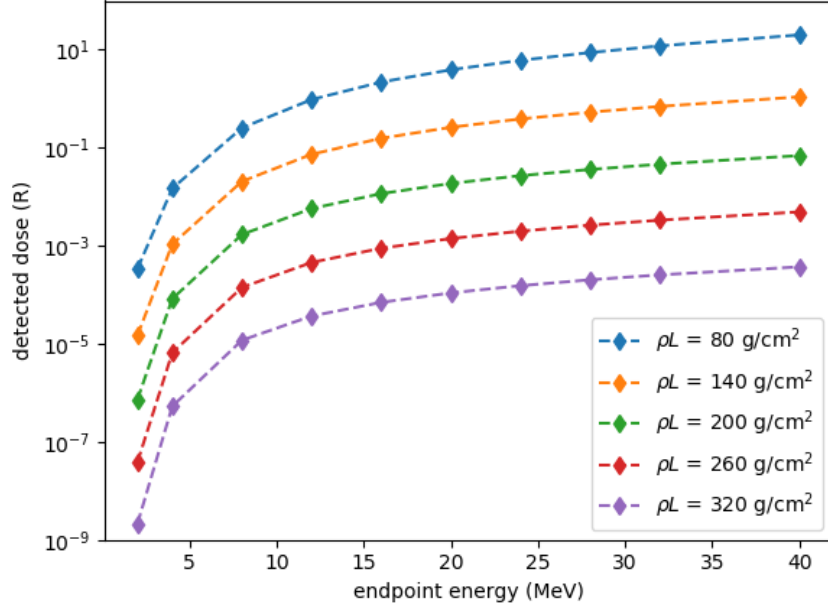


Figure 3. The detected direct flux as a function of scene thickness and electron beam energy.

The data in Figure 3 reveal that there is great advantage in increasing electron beam energy from 2 to 8 MeV. This is the motivation for MeV radiography—photoelectric and Compton interactions fall off dramatically in this range. However, the incremental advantage decreases above 10 MeV. The scaling in this range will be fit and compared to the oft-cited 2.8 power law.

Areal mass dependent power law scaling

Power law scaling is best revealed in log-log relationships, where these functional forms plot as straight lines. Figure 4 compares the dose as a function of endpoint energy to a 2.8 power scaling. The energy range in this particular figure is 2 to 16 MeV, and the slope of the interpolated data changes rapidly. As described earlier, this is due to the rapid decrease in photoelectric and Compton cross sections in the range of energies that correspond to the bulk of the flux contained in these spectra. At the highest energies plotted, an asymptotic behavior appears that begins to compare relatively well with the 2.8 power scaling. However, below this a much higher, and rapidly varying, exponent would be more appropriate.

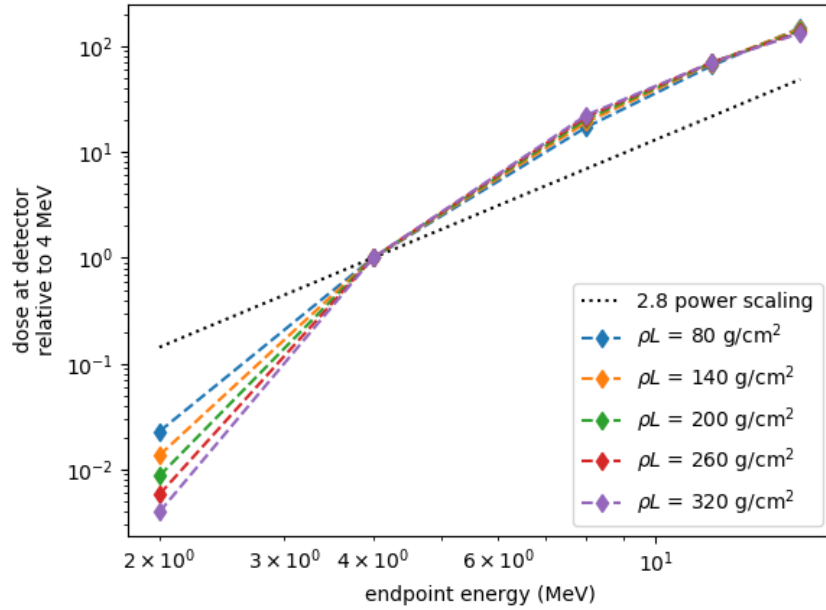


Figure 4. The log-log relationship between detected direct flux and electron beam energy during the transition from Compton-dominated to pair-production dominated scattering regimes.

Energies from 16 to 40 MeV are considered in Figure 5. In that range, the behavior appears much more linear in a log-log sense. All of the data are normalized to the signal level at 24 MeV, and are bounded by 2.8 and 1.54 power laws. This difference, the reduction in the power law scaling from 2.8 toward some lower asymptotic limit, is due to hardening of the spectrum and depends on the degree of that hardening, or the depth of the attenuation ‘window.’ Hardening, in turn, is a function of areal mass and atomic number. Therefore, given a particular atomic number, we propose that the signal due to unattenuated photons scale as,

$$\frac{S}{S_0} \propto \left(\frac{E}{E_0}\right)^{\alpha+\beta * \exp[-\gamma \rho L]} \quad (1)$$

In this form,

$$\lim_{\rho L \rightarrow 0} \left(\frac{S}{S_0}\right) \propto \left(\frac{E}{E_0}\right)^{\alpha+\beta} \cong \left(\frac{E}{E_0}\right)^{2.8} \quad (2)$$

In other words, the power law scaling of incident flux is recovered in the limit of zero density. The parameters α , β , and γ would need to be fit for the appropriate scene. Furthermore, because the log-log slope of relative signal vs. endpoint energy continues to change very slightly as the mean energy of the incident spectrum approaches and then begins to exceed the minimum in the attenuation curve, these parameters may also vary slightly depending on the energy range of interest. The expression is approximate, and does not substitute for more sophisticated modeling when high precision estimates are required.

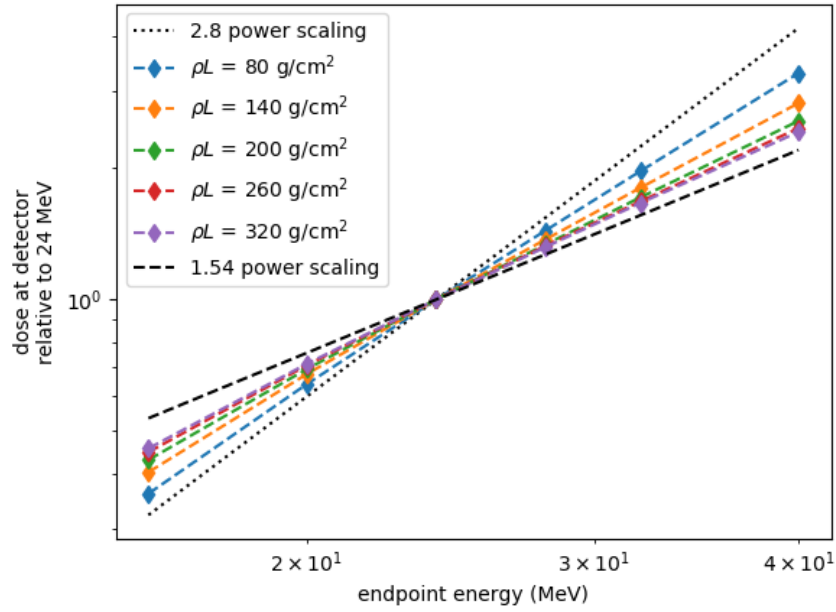


Figure 5. Detected direct flux vs. endpoint energy in the range of 16–40 MeV, where the log-log relationship is nearly linear with slope being a function of the degree of hardening in the scene.

Rearranging Eq. (1), the following expression is obtained:

$$\frac{s}{s_0} \propto \left(\frac{E}{E_0}\right)^{2.8} \left(\frac{E}{E_0}\right)^{-\beta(1-\exp[-\gamma\rho L])}. \quad (3)$$

Here again, the asymptotic limit is a 2.8 power law. Spectral hardening is contained entirely in the second multiplicative term, where β describes the strength of the effect in its large areal density limit, and γ scales the ρL dependence according to the material in the scene, including any filtering by low-Z materials along the line of sight that are not accounted in ρL . The simulation data are plotted again in Figure 7, this time with linear axes for ease of inspection. Again, note that all the data are bounded by the 2.8 and 1.54 power laws. These are the approximate asymptotic limits of Eq. (3) where β and γ have been fit as 1.258 and 6.38E-3, respectively. The first parameter, β , is dimensionless. The second parameter, γ , has units of effective cross section, cm^2/g . Areal densities in the middle of the range lie near a 2.0 power, or E^2 , curve.

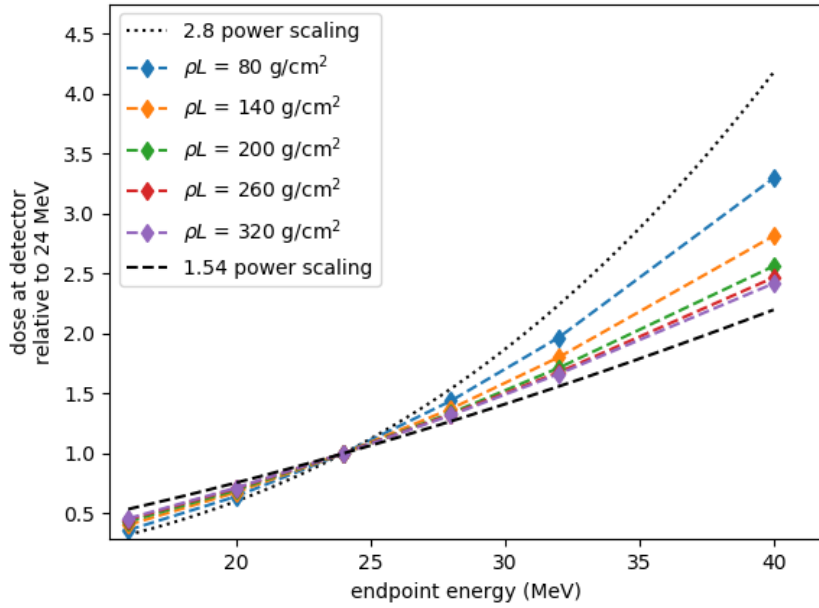


Figure 6. The data from Figure 5, re-plotted on linear-linear axes.

As noted earlier, the fitted expression is only approximate and subject to the condition that the data lie on a straight line in $\log(\text{dose})$ - $\log(\text{energy})$ space. For the data shown in Figure 6, the standard deviation of the error between fit and data is approximately 3.4%. This can be seen in Figure 7 where evaluations of Eq. (3) are plotted vs. the corresponding data.

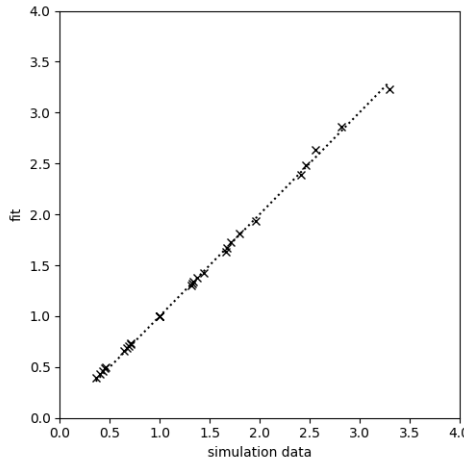


Figure 7. Evaluation of Eq. (3) compared to data so as to illustrate the quality of the approximation in the selected regime.

Summary

A modified radiographer's equation is presented that provides guidance as to the relative benefit of increasing electron beam energy for MeV radiography using bremsstrahlung sources. It includes a consideration of the material along the line of sight, and is dependent on the areal density of high-Z material in the scene. For a nominal radiographic test stand having a 24 MeV electron beam and 40 g/cm^2 of Al filtering the incident radiation, free parameters of the modified radiographer's equation are fitted and given

in the text above. They imply that, when attempting to penetrate 200 g/cm² of W, the signal, or intensity of the radiographic image, will scale not as E^{2.8}, but rather as E^{1.9}. This reduction in sensitivity to spectral endpoint energy is due to hardening of the radiation, or in other words increased attenuation at high energy due to pair production in W. This correction to the expected scaling should be accounted for in the optimization of beam energy and current during the design of new experiments and radiographic systems.

References

- [1] D. Venable, D.O. Dickman, J.N. Hardwick, et al., "PHERMEX: A Pulsed High-Energy Radiographic Machine Emitting X-Rays," LA-3241, 1967.
- [2] M. J. Burns, G. J. Caporaso, B. E. Carlsten, Y. J. Chen, K. P. Chow, E. G. Cook, H. A. Davis, C. A. Ekdahl, W. M. Fawley, C. M. Fortgang and T. P. Hughes, "Status of the dual axis radiographic hydrodynamic test (DARHT) facility," AIP Conference Proceedings, vol. 650, no. 1, pp. 139-142, 2002.
- [3] "ASD - Scorpius Conceptual Design Report," ECSE-RPT-CRD-0001, pp. 1-554., 2018.
- [4] C.D. Tomkins, B. Tobias, J.L. Carroll, J.L.S. Disterhaupt, J.O. Perry, Assessing Radiographic Performance of Scorpius Against Physics Requirements, LA-CP-18-20605 (2018)
- [5] A.R. Hawkins, S.A. Watson, and T.J. Kauppila, "Absolute Bremsstrahlung Energy Spectral and Dose Distributions – Theory and Experiment," M-4: GR-93-09, 1993
- [6] K. M. Hansen and G. S. Cunningham, "The Bayes Inference Engine," in Maximum Entropy and Bayesian Methods, 1996.